LOAD TRANSFER AT TRANSVERSE CRACKS IN CONTINUOUSLY REINFORCED CONCRETE PAVEMENT

Tatsuo Nishizawa
Associate Professor, Ishikawa National College of Technology

Shigeru Shimeno
Head of Pavement Section, Research Institute of Japan Highway Public Corporation

Akinori Komatsubara
Pavement Section, Research Institute of Japan Highway Public Corporation

Masashi Koyanagawa
Lecturer, Department of Agricultural Engineering, Tokyo University of Agriculture

ABSTRACT

In the structural design of continuously reinforced concrete pavement (CRCP), load transfer across transverse cracks should be properly taken into account. Finite Element Method (FEM) based on the elastic plate theory is a good tool for stress analysis of concrete pavement slab with joints and cracks. Though the load transfer across the cracks could be modeled by three elastic springs, it is difficult to determine the specific values of the spring constants. In this study, the values of the spring constants were backcalculated from the results of loading experiments conducted on test sections of CRCP. It was found that the backcalculated values depend on the temperature in the concrete slabs. The values were verified by comparing the strain predicted by FEM analysis with the measured ones. Effects of the spring constants on thermal strains were also examined.

INTRODUCTION

Continuously Reinforced Concrete Pavement (CRCP) has small transverse cracks with certain spacing which reduce the inner stresses due to volume change of concrete slab (1). However, these cracks change the structural characteristics of the concrete slab in carrying wheel loads. The rational thickness design of CRCP requires a mechanical model to calculate stresses in the concrete slab considering the load transfer across the transverse cracks. Finite Element Method (FEM) has been a powerful tool for the structural analysis of concrete pavements with joints and cracks(2,3,4,5). A mechanical FEM model for CRCP has been already developed by authors (6). In the model, a concrete slab with cracks is divided into rectangular plate elements and crack elements resting on a Winkler foundation and the load transfer across the cracks is modeled by a crack element with three elastic springs: shear, bending and torsion springs.

An essential point of the model is the determination of values of the spring constants representing the load transfer across the cracks. It has been recognized that narrow cracks in CRCP transfer a moment as well as a shear force (5). Therefore, values of the shear and bending spring constants should be properly specified in stress analysis of CRCP. Although we had derived a set of values of the spring constants from a result of a Benkelman beam test conducted on an old CRCP, these values had never been verified in terms of stresses in concrete slabs. Thus, more studies on the values of the spring constants has been required.

The purpose of this study is to estimate the values of the spring constants from measured strains obtained by a experiment conducted on full size pavements and evaluate effects of the values on strains due to wheel loads and curling deformations.

FEM ANALYSIS MODEL

Plate FEM Model

In this study, we employed a plate FEM model based on the theory of the elastic plate resting on a Winkler foundation as shown in Figure 1. The equilibrium equation of the model taking thermal strain into account can be expressed as follows (8):

$$(\mathbf{K}+\mathbf{J}+\mathbf{U}^{-1})\cdot\mathbf{d}_e=\mathbf{f}_s+\mathbf{f}_v-(\mathbf{J}+\mathbf{U}^{-1})\cdot\mathbf{d}_t \tag{1}$$

where,

$\mathbf{K}$: stiffness matrix of concrete slabs
$\mathbf{J}$: stiffness matrix of cracks
$\mathbf{U}$: flexible matrix of subbase
$\mathbf{d}_e$: displacement vector due to external force and self weight load
$\mathbf{f}_s$: external force vector
$\mathbf{f}_v$: self weight load vector
$\mathbf{d}_t$: displacement vector due to curling deformation
$\mathbf{d}_t$ at i-th node is written as follows:

$$\mathbf{d}_{ti}=\begin{Bmatrix} w_{ti} \\ \theta_{xti} \\ \theta_{yti} \end{Bmatrix}=\begin{Bmatrix} w_{ti} \\ -\dfrac{\partial w_{ti}}{\partial y} \\ \dfrac{\partial w_{ti}}{\partial x} \end{Bmatrix} \tag{2}$$

w_{ti} is the curling displacement at i-th node and can be estimated by the following equation.

$$w_{ti}=-\frac{3M_t}{4h^3E}(x_i^2+y_i^2) \tag{3}$$

where,

$$M_t=\alpha E\int_{-h/2}^{h/2} Tzdz \tag{4}$$

z: coordinate along the slab depth
α: coefficient of thermal expansion of concrete
T: temperature distribution in the slab
h: slab thickness
E : elastic modulus of concrete
x_i: x coordinate at i-th node
y_i: y coordinate at i-th node

We have developed an FEM system based on the theory mentioned above. The system consists of a CAD like mesh generator, an FEM solver and a graphical post-processor running on Windows system of personal computers. In this study, we used the system to calculate strains in concrete slabs.

Subbase Model

The Winkler foundation model is employed and modified to consider partial support of subbase. In this model, when some nodes of a concrete slab lift up from a subbase surface, the subbase support will be lost at these nodes. This can be formulated as follows:

$$q = \begin{cases} k \cdot (w - w_0) & \text{for } (w - w_0) \geq 0 \\ 0 & \text{for } (w - w_0) < 0 \end{cases} \quad (5)$$

where,

q: subbase reaction force
w: deflection of concrete slab
w_o: curling deformation of concrete slab
k: modulus of subbase reaction

Since the incorporation of Eq.(5) into Eq.(1) makes Eq.(1) nonlinear, Newton-Raphson method is employed to solve the nonlinear equation.

Crack Model

Load transfer across transverse cracks is modeled by a set of three elastic springs: shear, bending and torsion springs as shown in Figure 2. This model can be formulated as follows:

$$\mathbf{f}_l - \mathbf{f}_u = \mathbf{K}_J \cdot (\mathbf{d}_l - \mathbf{d}_u) \quad (6)$$

where,

$\mathbf{f}_l$, $\mathbf{f}_u$: resultant force vectors at loaded and unloaded nodes, respectively
$\mathbf{d}_l$, $\mathbf{d}_u$: displacement vectors at loaded and unloaded nodes, respectively

$$\mathbf{K}_J = \begin{bmatrix} \kappa_w & 0 & 0 \\ 0 & \kappa_t & 0 \\ 0 & 0 & \kappa_n \end{bmatrix} \quad (7)$$

κ_w, κ_t, κ_n: spring constants of shear, bending and torsion springs, respectively

In a previous study (6), values of the spring constants was derived from a measured deflection data of a Benkelman beam test conducted on an old CRCP. According to the study, load transfer across the transverse cracks is mainly carried by shear force. Moment transfer is supposed to exist only at very narrow cracks. Furthermore, torsion load transfer hardly exists and can be neglected in stress analysis. The study concluded that $\kappa_w = 5 \quad 10^3$ MPa, $\kappa_t = 10^5$ kN/m and $\kappa_n = 0$ kN/m.

However the conclusion has never been verified in terms of stresses in concrete pavement slab. Thus, in this study, we estimated the values of the spring constants based on the strains measured in test sections of CRCP.

Characteristics of Crack Model

To investigate the fundamental characteristics of the crack model, the effect of the spring constants on stresses in a concrete slab was numerically examined by FEM calculation. Table 1 shows the input data for the calculation which is based on a test section of a CRCP described in the later section. Values of the spring constants varied over wide ranges as shown in Table 2. Figure 3 shows a mesh used in the calculation. A load of 196 kN (20 tf) was applied at transverse crack edge. Longitudinal and transverse stresses (σ_y and σ_x, respectively) at loaded and unloaded nodes in the slab were calculated.

From the results of the calculation, it was found that the effect of κ_w on the transverse stress , σ_y, is most significant as shown in Figure 4. When κ_w is small and the shear transfer ability across the cracks is poor, σ_y is much greater at the loaded node than at the unloaded node. Increasing κ_w reduces the difference in σ_y between the loaded and unloaded node. When the value of κ_w is greater than 1×10^5 MPa, σ_y at the loaded and unloaded nodes are almost the same. The effect of κ_n appears in the figure, only if the value is greater than 1×10^7 kN/m. Narrow bands in the figure indicate the effect of κ_t which is relatively small.

On the other hand, the longitudinal stress, σ_x, is mostly affected by κ_t as shown in Figure 5. It is because the bending spring transfers a moment which induces longitudinal bending stress. When κ_t is less than 1×10^5 kN/m, σ_x at the loaded and unloaded nodes are almost zero. σ_x increases as κ_t increases and eventually converges to a certain level. The value of κ_n little affects σ_x in the range considered. The effect of κ_w appears as very narrow bands in the figure.

Table 2 summarizes the ranges of the values which affect the stresses in the concrete slab. In the range of $\kappa_w > 1\times10^6$ MPa, $\kappa_t > 1\times10^9$ kN/m and $\kappa_n > 1\times10^7$ kN/m, the stresses are about the same as ones when there is no transverse crack.

STRAIN AND TEMPERATURE MEASUREMENTS ON TEST SECTIONS

Overview of Test Sections

Load induced strains and temperatures in concrete slab were measured on test sections of CRCP. The test sections are on a road connecting Suita and Yamaguchi of Sanyo Express Highway. Two types of cross section, namely Section A and Section B, were selected. Table 3 presents dimensions of the concrete slabs, steel reinforcements and concrete and subbase properties which were obtained from laboratory tests and plate loading tests. Since Section A was on a climbing lane, the width of concrete slab is relatively small (3m). Strain gauges with thermometer were installed in the concrete slabs, as shown in Figure 6. At each measurement point, three gauges were embedded at top, mid-depth and bottom of the slabs.

The test sections had been constructed in November, 1995. When the first measurements were conducted three months after the construction, transverse cracks were observed as shown in Figure 6. The openings of the cracks were very narrow (less than 0.1 mm). Crack patterns on the test sections had not changed during the tests.

Loading Test

Loading tests were conducted on the test sections in a late winter (Section A: March 5, Section B: February 15) and in a spring (Section A: May 14, Section B: April 25). A load was applied through a steel plate with a diameter of 300 mm and an oil jack. Loading positions were interior (No.1 in Figure 6) , free-edge (No.2), crack-edge (No.3) and crack-corner (No.4). In a loading process, magnitude of the load was increased with an increment of 9.8 kN (1 tf) and strains and temperatures were measured at every load increment. When a reading of the gauge under the loading plate became about 10^{-4} or the magnitude of the load reached the maximum of 196 kN (20tf), the oil of the jack was released. This loading process was repeated three times to check the reproduction of response at each loading position.

Figure 7 shows a typical example of load-strain curve obtained at the first loading test (late winter) in Section A. As can be seen, load-strain curves are linear and the absolute values of the strains at the top and bottom gauges are almost the same and their signs are opposite, which agrees to the response of the linear elastic plate theory.

Table 4 summarizes average temperatures and temperature differentials between the top and bottom of the concrete slab in each loading test. It is apparent that the average temperatures and the temperature differentials were less at the first loading test than at the second loading test.

Figure 8 shows the differences in the measured strains under the loading plate in the first and second tests. It is apparent that there is little difference in the strains of the interior and free-edge loading conditions, whereas great difference can be seen in the strains of the crack-edge and crack-corner loading conditions. This would be due to the difference in the temperature of the slabs. In high temperature conditions, the crack opening is narrow and the load transfer efficiency is high, leading to stresses near the crack decreasing.

Measurement of Thermal Strain

To investigate the thermal strains, before each loading test, temperatures and strains of the embedded gauges were measured at every one hour for about two weeks. Since the slab width of Section A is smaller than that of normal pavements, the conditions of the restraint is expected to be a little different from normal pavements. Therefore, data obtained in Section B will be discussed in the following. Figure 9 shows an example of the temperature and strain changes in Section B at the first measurement (late winter). Strains plotted in the figure are the restrained ones, which are estimated as follows:

$$\varepsilon_r = \varepsilon_m - \alpha \cdot t \tag{8}$$

where,

ε_r : restrained strain in concrete slab
ε_m : measured strain in concrete slab
α : thermal coefficient of expansion of concrete (=10^{-5}/°C)
t : temperature change from a reference temperature when temperature differential is zero.

The restrained strains are plotted as positive value when they are tensile. In the daytime, since temperature is high but the concrete slab can not expand freely because of the restraint due to the friction between concrete slab and subbase, the restrained strains appear as negative value. Thus, trends of the change of temperature and strain are opposite. This can be clearly seen in Figure 9.

Figure 10 shows daily changes of temperature and strain distributions along the slab depth. In the daytime, temperatures at the top surface is higher than at the bottom, and in the night time it is opposite. On the contrary, restrained strain at the top surface is lower than at the bottom in the daytime. This means that thermal stress due to the temperature gradient is tensile at the bottom surface in the daytime.

Distributions of temperature and strain are assumed to be a function of z, $f(z)$, and to be divided into axial, curling and nonlinear components as follows:

$$f(z) = a + \phi \cdot z + g(z) \tag{9}$$

where,
a : axial component
ϕ : gradient
z : coordinate along the slab thickness
$g(z)$: nonlinear component

Then, assuming $f(z)$ to be a quadratic function of z (7), three constants of the function can be determined form the data measured at the top, mid-depth and bottom gauges. Since $a + \phi \cdot z$ is a linear function of z, two constants of the function can be determined from the following conditions:

$$\begin{aligned} \int_A g(z)dz &= \int_A \{f(z) - a - \phi \cdot z\} dz = 0 \\ \int_A g(z)zdz &= \int_A \{f(z) - a - \phi \cdot z\} zdz = 0 \end{aligned} \tag{10}$$

In the later section, axial and curling components are discussed in terms of the restrained strain.

ANALYSIS OF STRAIN DUE TO LOAD

Interior and Free Edge Loading Conditions

To verify the FEM analysis, FEM calculation was performed for the interior and free-edge loading conditions where the effects of the load transfer across the cracks are small. Properties of the concrete slabs and the subbases presented in Table 2 were used in the calculation. Mesh for each test section is shown in Figure 11.

Figure 12 shows a comparison between the measured and calculated strains in the interior and free-edge loading conditions, indicating that the agreement is fairly good. The average error between the measured and calculated strains is evaluated by the following equation:

$$e_s = \sqrt{\frac{1}{n}\sum_{i=1}^{n}(\varepsilon_i^m - \varepsilon_i^c)^2} \tag{11}$$

where,

e_s : average error($\times 10^{-6}$)
n : number of strains compared
ε_i^m : measured strain
ε_i^c : calculated strain

For the case of Figure 12, e_s is calculated to be 13.2, which can be considered to represent an accuracy of the FEM analysis.

Crack Edge and Crack Corner Loading Conditions

Based on the measured strains, the values of the spring constants of transverse crack were backcalculated using the FEM model. A number of calculations were performed varying the values of the spring constants as shown in Table 5. From the strains calculated for all combinations of the values and the corresponding measured strains, e_s was calculated for each case. A combination of the values was taken if e_s is less than 13.2 or is the minimum.

Table 6 summarizes the backcalculated values of the spring constants. e_s in the crack edge loading is less than 13.2 and thus the agreement is good. However, e_s of the corner loading is much greater than 13.2 in most cases. Since the crack-edge loading condition is considered to be critical in the thickness design of CRCP, the values obtained in that condition are discussed in the following. The backcalculated values of the spring constants have a wide range, since the errors in the measurement and the model can not be avoidable. Particularly, κ_n is backcalculated in a quite wide range, since its value little affects the stress near the cracks as previously mentioned. The values of κ_w and κ_t obtained in the previous study fall (6) in the range backcalculated in this study.

Figure 13 shows a comparison between the strains calculated using the backcalculated values and the measured strains. In the FEM calculation, the minimum values for the spring constants were taken if they have a range. It can be seen that the agreement is quite good.

It seems that these values vary with the temperature of the slabs at the time of loading test. Figure 14 shows the relationships between the values of the spring constants and the average temperature in the concrete slabs. When the temperature is high, except κ_t in the section B, the values of κ_t and κ_w increase. It is because the opening of crack is small if temperature in concrete slab is high, leading to high load transfer efficiency.

It would be unrealistic that, in the fatigue analysis for the thickness design, the values of the spring constants are changed depending on the temperature in concrete slab . Therefore, the low values of κ_w=5×10^4 MPa and κ_t =1×10^7 kN/m and κ_n = 0 kN/m are recommended in the stress calculation for the design.

ANALYSIS OF STRAIN DUE TO TEMPERATURE

Axial Component

Figure 15 shows the relationships between axial component of restrained strain, ε_a, and axial component of temperature, t_a, in Section B. s7, s8, s13 and s14 in the figure denote the gauge ID of which positions are shown in Figure 6. If horizontal movement of a concrete slab is completely restrained, ε_a would linearly decrease with temperature. On the contrary, if the slab can freely move, ε_a would be zero independent from temperature. ε_a of s7 and s13 which are placed in the longitudinal direction linearly decrease with temperature. This means that the concrete slab was longitudinally restrained. But this trend is much stronger at the second measurement than at the first measurement. ε_a of s8 and s14 which are placed in transverse direction are almost zero, meaning that the slab could freely move in the transverse direction. Thus, the restrained stress in the transverse direction could be neglected in the design.

Curling Component

Figure 16 shows the relationships between the gradient of the restrained strain, ϕ_ε, and the gradient of temperature, ϕ_t, of the gauges of s7, s8, s13 and s14 in Section B. Positive values of ϕ_ε or ϕ_t indicate that value at the bottom is greater than at the top. So positive ϕ_ε causes the tensile stress at the bottom surface of the concrete slab. Marks indicate measured ϕ_ε and lines were obtained by the FEM calculation using three sets of κ_w and κ_t as presented in the figure. Although the measured data have some scattering, it can be seen that ϕ_ε increases as ϕ_t increases. Increasing values of κ_w and κ_t increases the degree of restraint and thus increases the values of ϕ_ε. The effect of κ_w and κ_t is greater on the longitudinal strains near the crack (s7) than those far away from the crack (s13). The effect is little in the transverse strains (s8 and s14). Measured strains agree to the calculated ones, when the values of κ_w and κ_t are large. Thus, in estimating curling stress, it could be recommended to use large values of spring constants.

CONCLUSIONS

For the thickness design of CRCP, a FEM model based on the elastic plate resting on a Winkler foundation was developed. The essential point of the model is the determination of value of the spring constants representing the load transfer across the cracks. In this study, the values were backcalculated from the measured strains obtained by the full scale pavement experiment. These values were found to have a range and depend on the average temperature in concrete slab. However, specific values should be selected for the thickness design. For that, it is proposed that, in the calculation of load stress, minimum values: $\kappa_w=5\ 10^3$ MPa and $\kappa_t=1\ 10^7$ kN/m and $\kappa_n=0$ kN/m, could be used, whereas, in the calculation of curling stress, maximum values: $\kappa_w=1\ 10^7$ MPa, $\kappa_t=1\ 10^9$ kN/m and $\kappa_n=0$ kN/m, could be used.

LIST OF FIGURES

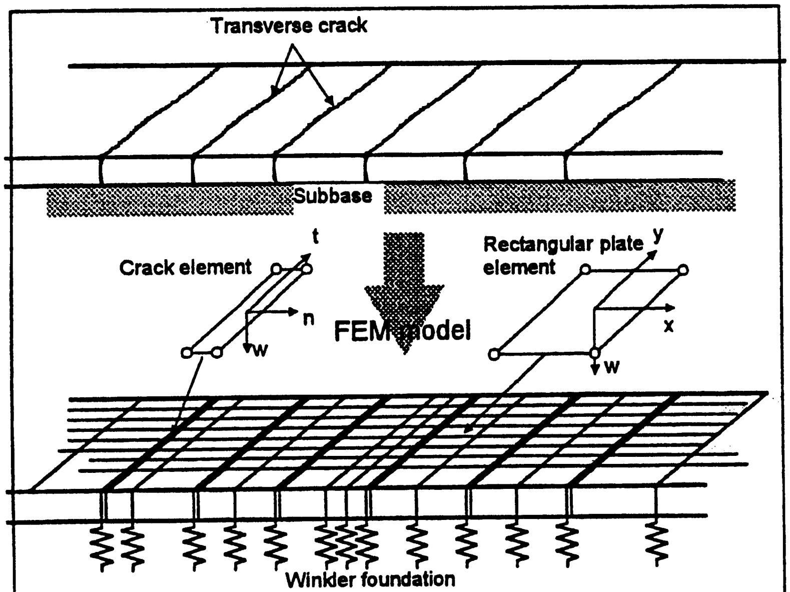

FIGURE 1 FEM model for CRCP

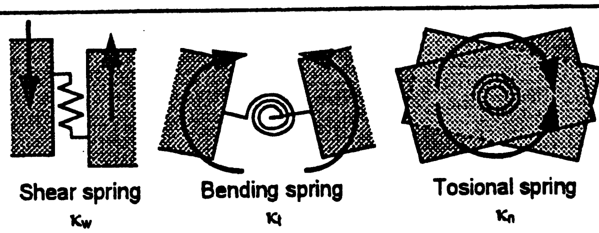

FIGURE 2 Spring model for load transfer across the crack

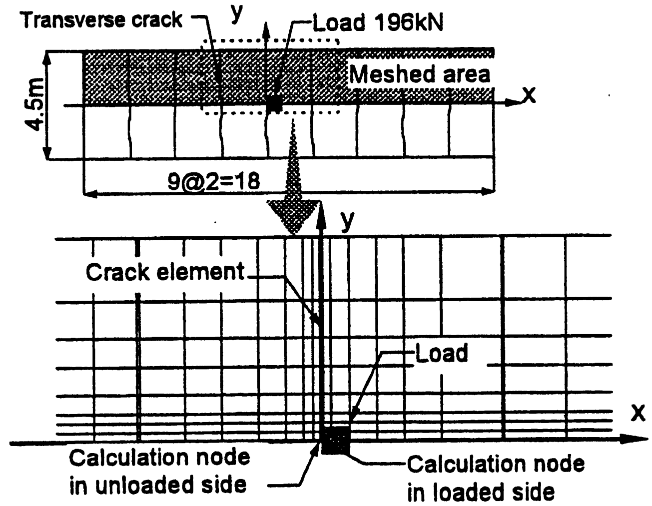

FIGURE 3 Mesh layout for crack edge loading condition

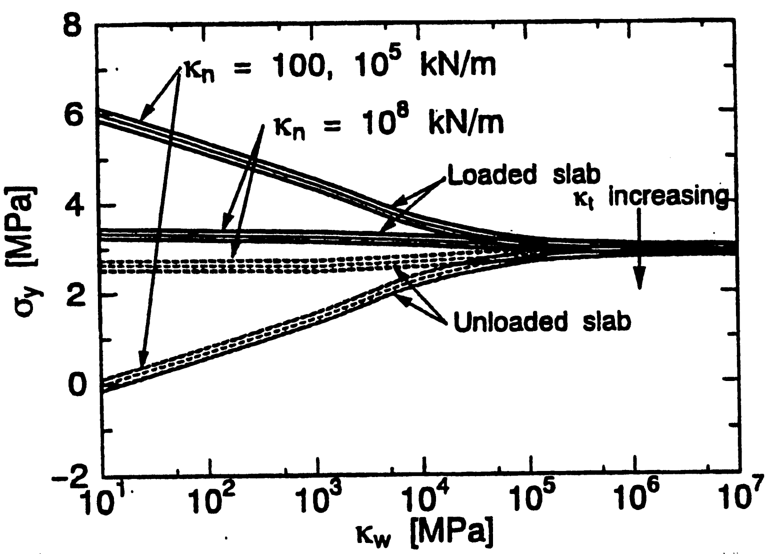

FIGURE 4 Effect of spring constants on transverse stress

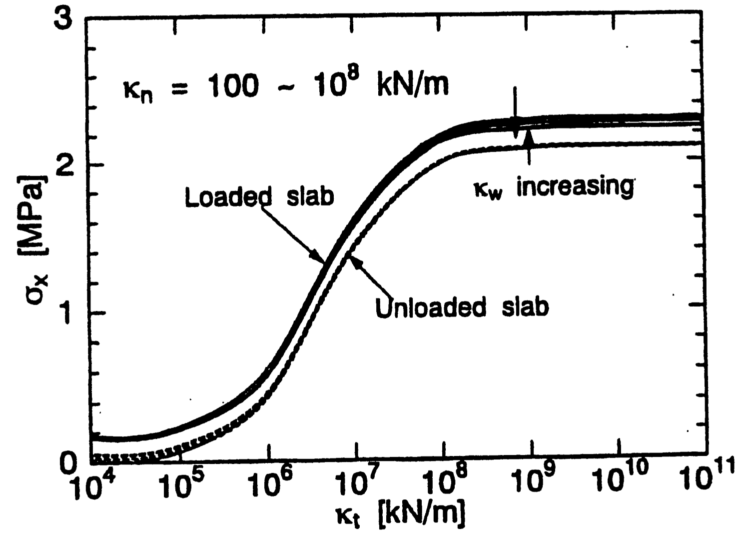

FIGURE 5 Effect of spring constants on longitudinal stress

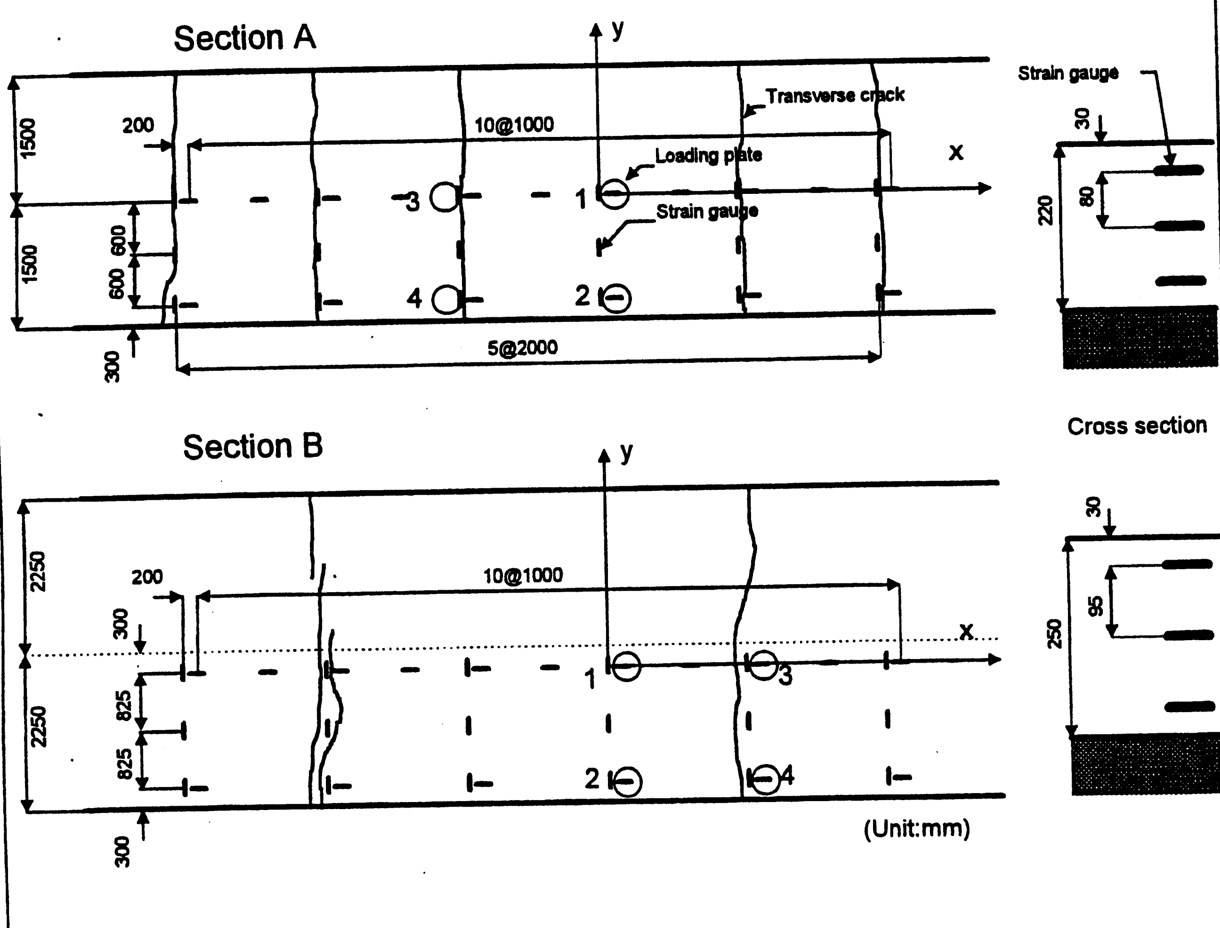

FIGURE 6 Installation of strain gauges and loading positions

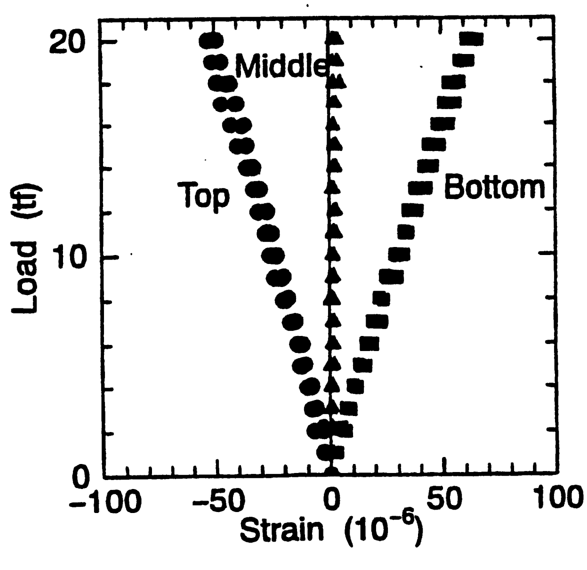

FIGURE 7 An example of load-strain curves obtained from the first loading test (s13 in Section A)

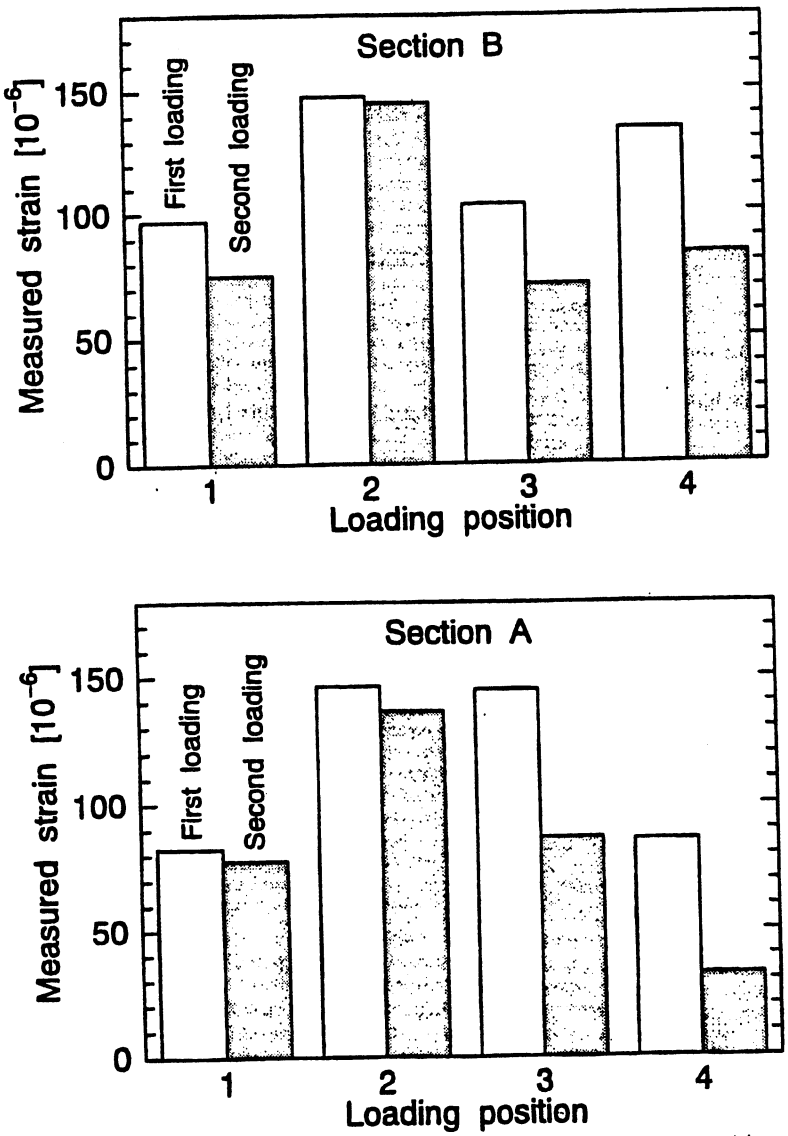

FIGURE 8 Difference of strains under the loading plate between the loading times

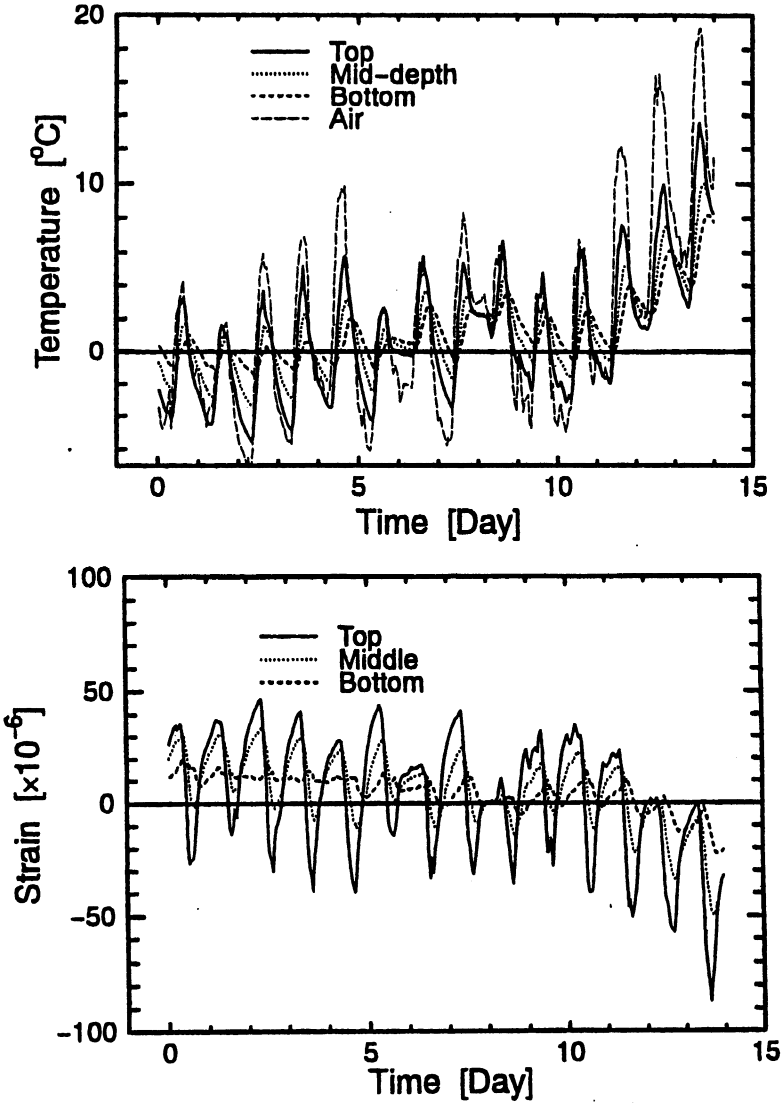

FIGURE 9 An example of measured changes of temperatures and restrained strains (s13 in Section B)

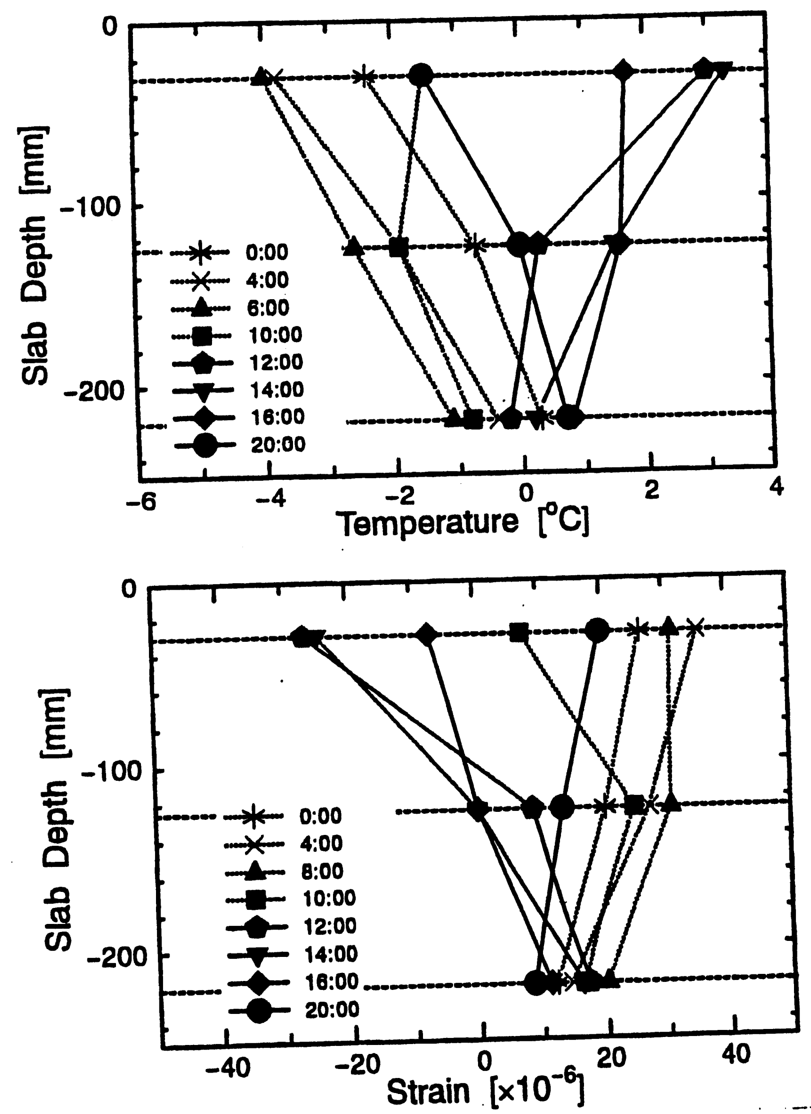

FIGURE 10 An example of measured distributions of temperature and restrained strain through the slab depth (s13 in Section B)

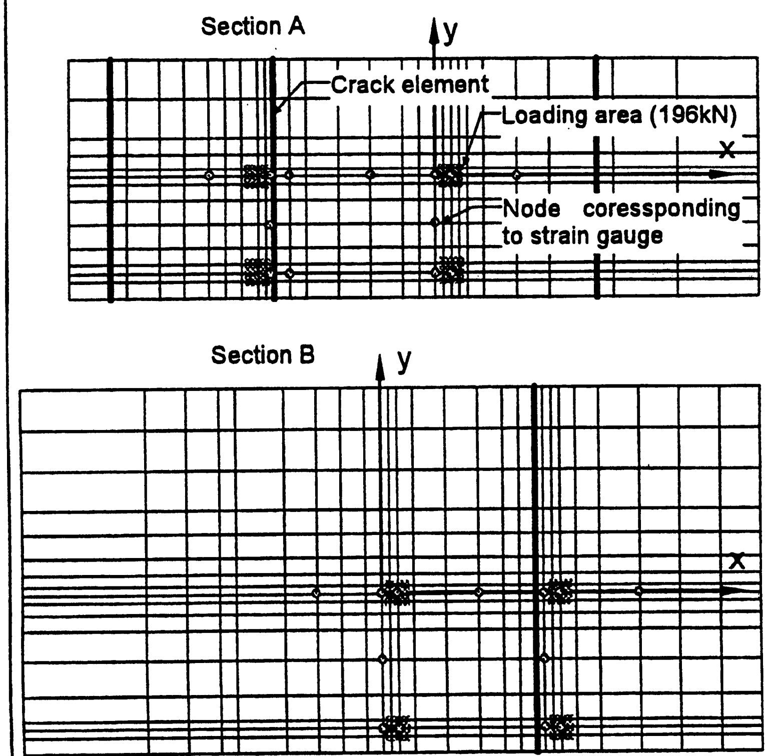

FIGURE 11 Mesh layouts for the analysis of the loading tests

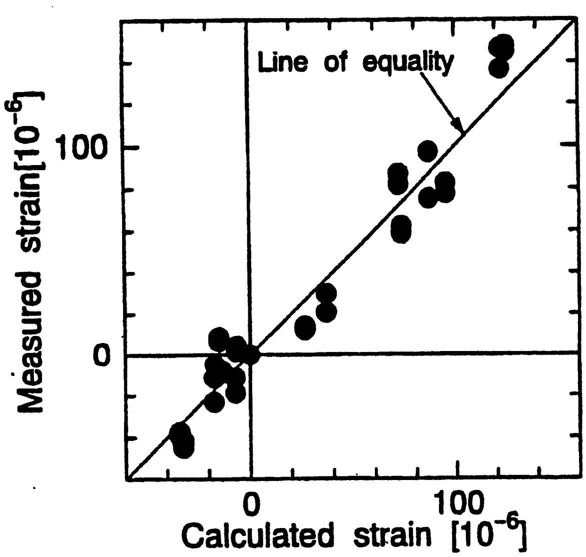

FIGURE 12 Comparison of strain for the interior and free edge loading conditions

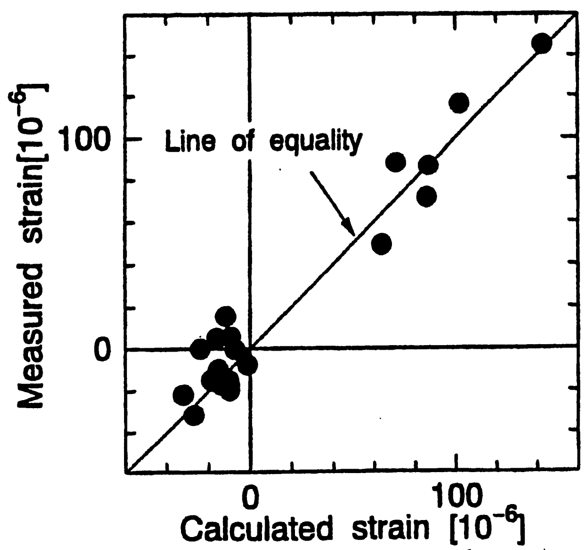

FIGURE 13 Comparison of strain for the crack edge and crack corner loading conditions

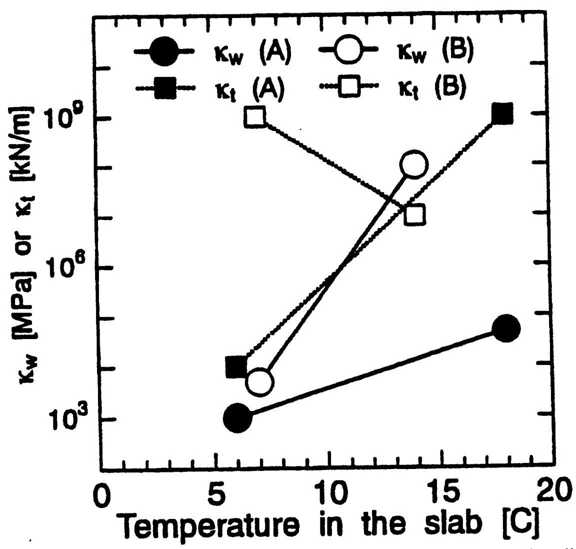

FIGURE 14 Effects of temperature in concrete slab on the values of spring constants

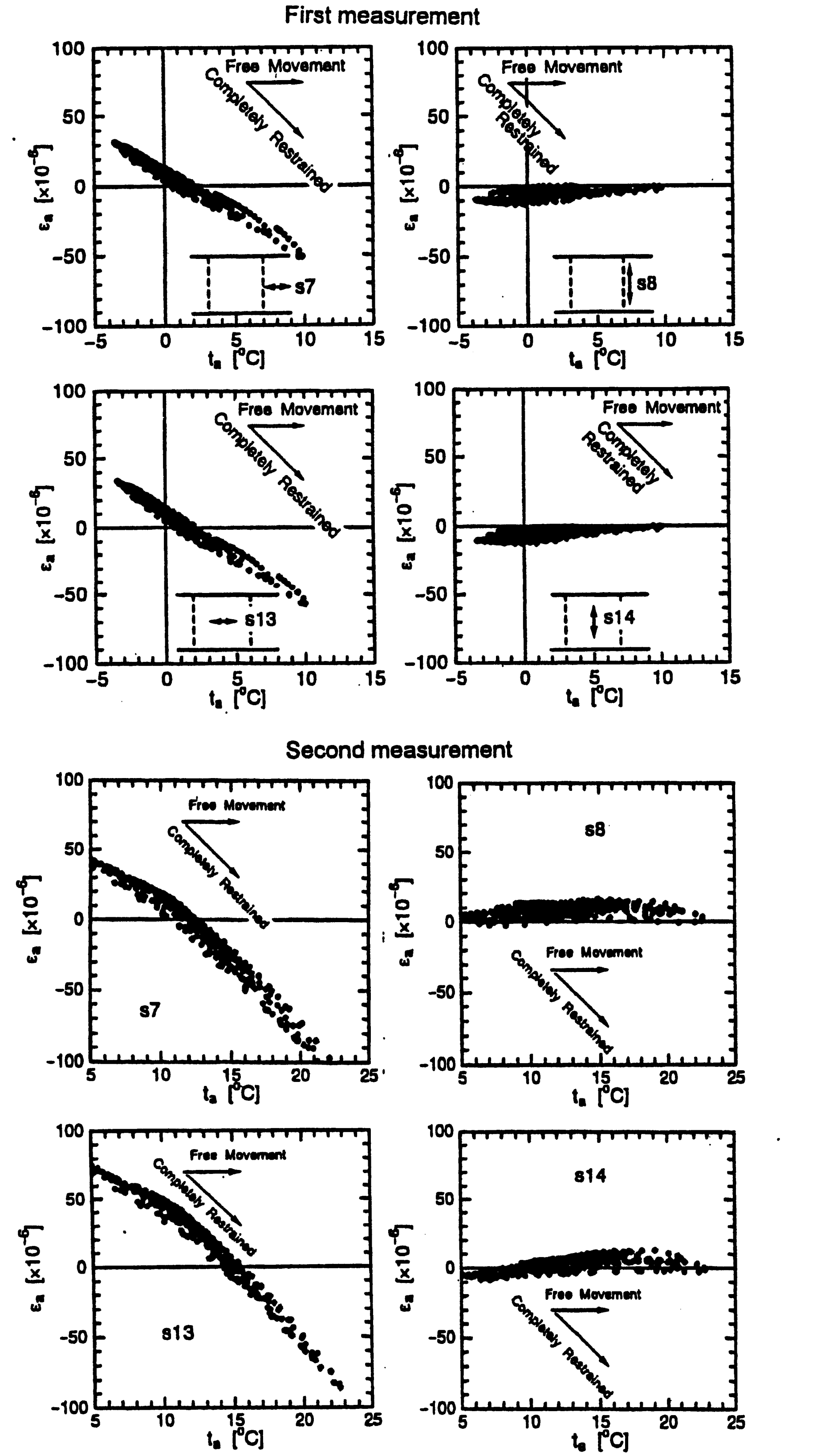

FIGURE 15 Relationships between axial temperature t_a and axial restrained strain ε_a (Section B)

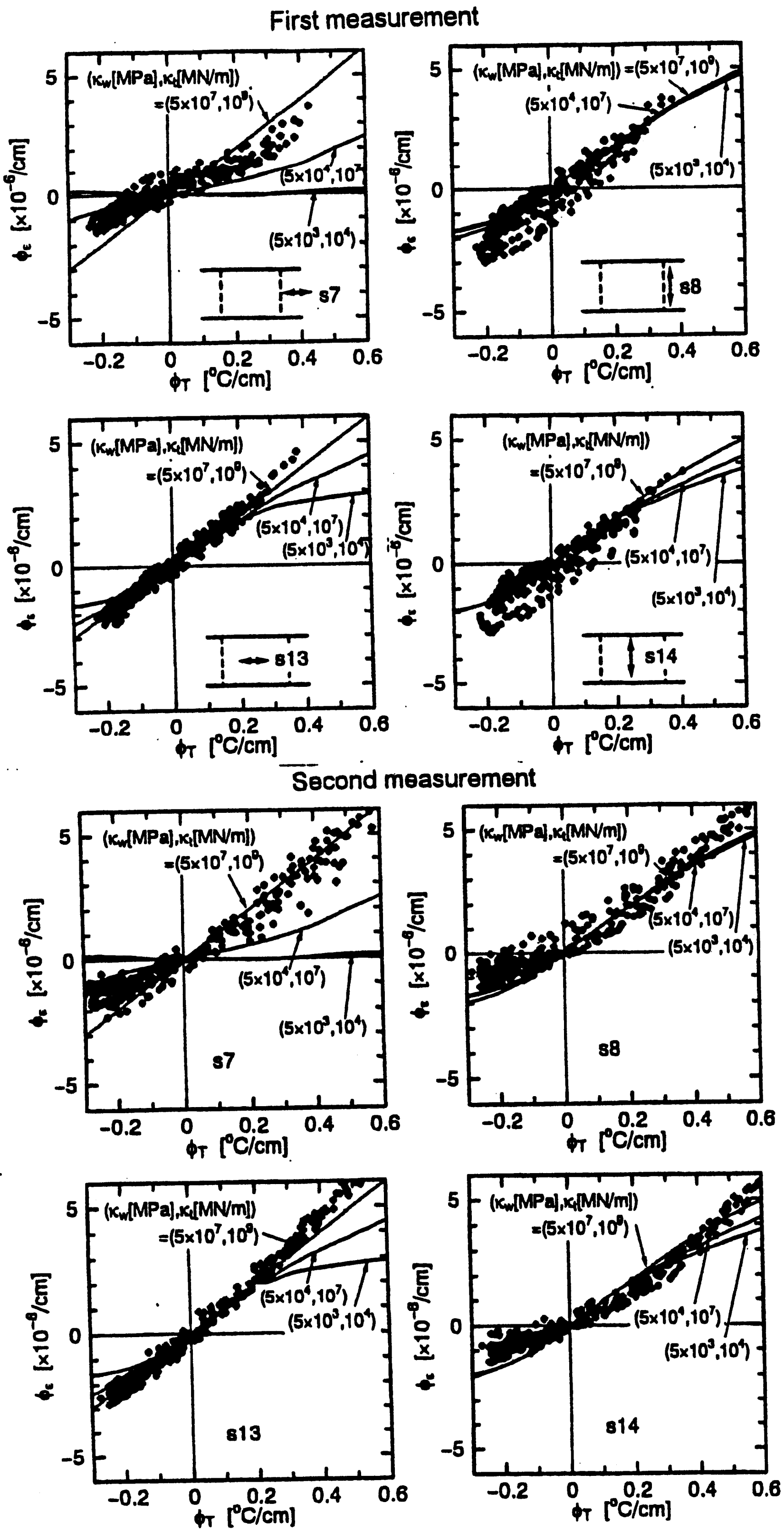

FIGURE 16 Relationships between temperature gradient ϕ_T and gradient of restrained strain ϕ_ε (Section B)

LIST OF TABLES

TABLE 1 Input data for crack edge loading condition

Property	Value
Width of concrete slab (m)	4.5
Thickness of concrete slab (mm)	250
Elastic modulus of concrete (GPa)	34
Poisson ratio of concrete	0.13
Shear spring constant (MPa)	1.010^{1}~1.010^{7}
Bending spring constant (kN/m)	1.010^{4}~1.010^{11}
Torsion spring constant (kN/m)	1.010^{2}~1.010^{8}
Spacing of transverse cracks (m)	2
Modulus of subbase reaction (kN/m^3)	191

TABLE 2 Effective ranges of the spring constants on concrete stresses

Spring constant	Range of value	Stress affected
κ_w (MPa)	~1.010^{5}	Stress parallel to crack
κ_t (kN/m)	1.010^{5}~1.010^{9}	Stress perpendicular to crack
κ_n (kN/m)	1.010^{7}~	Stress parallel to crack

TABLE 3 Properties of the test sections of CRCP

Property	Section A	Section B
Concrete slab		
Width (m)	3.0	4.5
Thickness (mm)	220	250
Spacing of longitudinal steel (ctc D16,mm)	150	125
Amount of Longitudinal steel (%)	0.6	0.64
Spacing of transverse steel (ctc D16,mm)	500	500
Elastic modulus (GPa)	30.1	34.7
Poisson's ratio	0.137	0.134
Subbase		
Thickness of cement treated subbase (mm)	150	150
Modulus of subbase reaction (kN/m^3, with 300mm diameter plate)	1823	421

TABLE 4 Temperatures of concrete slab at the time of the loading tests(°C)

Loading position	Average	Differential	Average	Differential
Section A				
	First loading		Second loading	
1	6	2	23	6
2	4	1	23	3
3	6	1	18	4
4	7	1	21	2
Section B				
	First loading		Second loading	
1	6	2	23	6
2	4	1	23	3
3	6	1	18	4
4	7	1	21	2

TABLE 5 Values of spring constants for the back-calculation

κ_w (MPa)	110^3, 510^3, 110^4, 510^4, 110^5, 110^8
κ_t (kN/m)	110^4, 510^4, 110^5, 510^5, 110^6, 110^7, 110^9,
κ_n (kN/m)	0, 110^3, 110^4, 110^5, 110^6, 110^7, 110^9,

TABLE 6 Results of the back-calculation of spring constants

Loading Position		κ_w (MPa)	κ_t (kN/m)	κ_n (kN/m)	es
Section A					
3	First loading	110^3	110^3~110^5	110^6	12.3
	Second loading	510^4~110^6	110^3	0~110^6	12.9
4	First loading	110^3	110^6	0~110^6	8.3
	Second loading	110^8	110^9	0~110^6	21.7
Section B					
3	First loading	510^3	110^9	0~110^6	12.9
	Second loading	110^8	110^7	0~110^6	12.3
4	First loading	510^4~110^6	110^9	0~110^9	35.6
	Second loading	510^4~110^8	110^6~110^7	0~110^9	24.1

REFERENCES

1. McCullough, B.F., Criteria for the Design and Construction of Continuously Reinforced Concrete Pavement, In *Concrete Pavements* edited by A.F.Stock, Elsver Applied Science, New York, pp.279-318, 1988.

2. Tabatabaie, A.M., and E.J. Barenberg, Structural Analysis of Concrete Pavement System, *Journal of Transportation Engineering*, ASCE, Vol.106, No. TE5, pp.493-506, 1980.

3. Huang, Y.H., A Computer Package for Structural Analysis of Concrete Pavements, *Proceedings, 3rd International Conference on Concrete Pavement Design and Rehabilitation*, Purdue University, pp.295-308, 1985.

4. Ioannides, A.M., M.R. Thompson, and E.J. Barenberg, Finite Element Analysis of Slab-on-Grade Using Support Models, *Proceedings, 3rd International Conference on Concrete Pavement Design and Rehabilitation*, Purdue University, pp.309-324, 1985.

5. Majidzadeh, K., G.J. Ilves, and H. Sklyut, RISC - A Mechanistic Method of Rigid Pavement Design, *Proceedings, 3rd International Conference on Concrete Pavement Design and Rehabilitation*, Purdue University, pp.341-350, 1985.

6. Nishizawa, T., S. Matsuno, and T. Fukuda, A mechanical Model for Rational Design of CRCP, *Proceedings, 3rd International Conference on Concrete Pavement Design and Rehabilitation*, Purdue University, pp.431-443, 1985.

7. Jakson, P.A., Continuously Reinforced Concrete Pavement: A Literature Review, *Contractor Report 127*, transport and Road Research Laboratory, pp. 17-21.

8. Nishizawa, T., T. Fukuda, S. Matsuno, and K. Himeno, Curling Stress Equation for Transverse Joint Edge of Concrete Pavement Slab Based on FEM Analysis, *Transportation Research Record 1525*, Transportation Research Board, pp. 35-43, 1996.

9. Choubane, B., and M. Tia, Analysis and Verification of Thermal Gradient Effects on Concrete Pavement, *Journal of Transportation Engineering*, ASCE, Vol. 121, No.1, pp.75-81, 1995.